Computer-simulation studies of intrinsic defects in $LiNbO_3$ crystals

H. Donnerberg
Department of Physics, University of Osnabrück, D-4500 Osnabrück, West Germany

S. M. Tomlinson and C. R. A. Catlow
Department of Chemistry, University of Keele, Keele, Staffordshire ST5 5BG, United Kingdom

O. F. Schirmer
Department of Physics, University of Osnabrück, D-4500 Osnabrück, West Germany
(Received 27 January 1989)

We have performed an atomistic simulation study of the defect structure of $LiNbO_3$ crystals resulting from Li_2O deficiency and reduction treatments. Li_2O excess is found to be unlikely in $LiNbO_3$ crystals. It is shown that oxygen vacancies are not the dominant intrinsic defect species in $LiNbO_3$. Important defects are $(Nb^{4\cdot}_{Li}V^{5'}_{Nb})'$ and isolated $Nb^{4\cdot}_{Li}$ antisites. Small regions of $LiNbO_3$ with ilmenite-like cation-stacking sequence are likely to occur; thus $(Nb^{4\cdot}_{Li}V^{5'}_{Nb})'$ defects in $LiNbO_3$ should be interpreted as Li vacancies within ilmenite-like crystal regions. Li Frenkel disorder is energetically favorable. Finally we study charge–self-trapping centers, i.e., polarons and bipolarons.

I. INTRODUCTION

Lithium niobate ($LiNbO_3$) is a ferroelectric material which does not occur naturally. Its large pyroelectric, piezoelectric, electro-optic, and photoelastic coefficients have made $LiNbO_3$ an important material for many different technical applications.

Numerous investigations on the structure and chemical composition of $LiNbO_3$ have revealed the high degree of ionic disorder and Li_2O deficiency in most analyzed $LiNbO_3$ crystals. It has been found that many physical properties, for example the extraordinary refractive index, birefringence, the linear electro-optical effect, and the Curie temperature depend to a certain extent on the intrinsic defect structure (see Refs. 1–4 for further references). Although careful experimental investigations of the intrinsic defect structure have brought some insight into a microscopic understanding, there is no general agreement upon one defect model. Related to this, considerable controversy exists about the occurrence of oxygen vacancies in $LiNbO_3$ as a defect resulting from reduction treatments.

In the case of perovskites, deviations from stoichiometry are accommodated by the formation of vacancies.[5,6] In addition, density measurements on reduced $SrTiO_3$ confirm that oxygen vacancies are the favored products of reduction,[7] as would be expected for crystals with perovskite structure.

It appears to be straightforward to extend this defect chemical behavior to $LiNbO_3$ because of its resemblance to the perovskites. Fay, Alford, and Dess[8] suggested in 1968 that Li_2O deficiency in $LiNbO_3$ is accommodated by the formation of Li and O vacancies. Jorgensen and Bartlett interpreted their conductivity measurements on reduced $LiNbO_3$ crystals in terms of oxygen vacancies.[9]

However, some experimental evidence does not support these simple defect models. First, the crystal density increases with increasing Li_2O deficiency[10] and degree of reduction,[6] whereas the purely subtractive defect models would require a decreasing density. Secondly, Abrahams and Marsh[11] showed by careful x-ray analysis of congruent $LiNbO_3$ that about 5.9% of the Li sites are occupied by Nb and 4.7% of the Nb sites are vacant. In addition, they showed that the oxygen sublattice is completely filled. Based on ^{93}Nb nuclear-magnetic-resonance studies Peterson and Carnevale[12] observed about 6% of the Nb in a different crystalline environment. Because of these results more elaborate models of Li_2O deficiency and reduction have been suggested, in which defects occur on the cation sublattice only, and small regions of ilmenite-like crystal structure are proposed to exist.[11,13] However, the defect chemistry governing reduction is still in question; Sweeney and Halliburton[14–16] have reported that an optical absorption band appearing at 500 nm by reduction disappears after an optical bleach at 80 K and is replaced by an absorption band near 760 nm. This in turn is correlated with a Nb^{4+} ESR signal. After the optical bleaching the 500-nm band can be restored upon warming the crystal from 80 to about 200 K. At the same time the 760-nm band disappears.

Essentially two explanations for these observations have been given: the interpretation of Sweeney and Halliburton is in terms of the oxygen-vacancy model, where the 500-nm band corresponds to internal transitions of the neutral vacancy and similarly the 760-nm band is assigned to the singly ionized vacancy. The attribution of the 760-nm band to Nb^{4+} optical absorption according to small-polaron theory could not be ruled out, and is generally accepted to be the origin of this absorption band (e.g., Ref. 17).

The second model suggested by Schirmer *et al.*[18] is purely polaronic. As above, the 760-nm band is attributed to single Nb^{4+} polarons, whereas the 500-nm band is

associated with bipolarons which consist of two neighboring polarons bound by means of lattice relaxation and covalency.

Recently Agulló-Lopez *et al.* investigated $LiNbO_3$ crystals of different compositions irradiated with high-energy electrons.[19] Optical absorption at 500 nm is observed to increase rapidly above 1.1 MeV electron-beam energy. From this threshold energy the authors infer oxygen-ion–displacement damage to be involved and ascribe the increasing optical absorption to oxygen vacancies. The similarity of the optical absorption after electron irradiation and reduction leads the investigators to conclude that oxygen vacancies are the dominant defect species after reduction.

The purpose of our theoretical contribution is to study the defect chemistry of $LiNbO_3$ using computer-simulation techniques. Our investigations concern the defect structure as a consequence of Li_2O deficiency and reduction treatments, and the possibility of small polarons and bipolarons. Moreover, studies on the mode of impurity incorporation are in progress and will be published later.

II. COMPUTATIONAL TECHNIQUES

Our calculations are based on an ionic description of the crystal, including the shell model proposed by Dick and Overhauser.[20] Crystal ions are thought to consist of an ion core (charge X and mass M) to which the electron shell (charge Y and mass 0) is coupled via a harmonic restoring force with spring constant K. The formal ionic charge is then given by $Q=X+Y$ and ionic polarizability by

$$a=Y^2/K \ . \tag{2.1}$$

The most important interactions between different ions are Coulomb forces and short-range Buckingham potentials which describe effects of the Pauli exclusion principle and electron correlation. Buckingham potentials are given by

$$V(r)=Ae^{-r/\rho}-C/r^6 \ . \tag{2.2}$$

The unknown parameters A, ρ, and C for each ion-ion potential and the shell parameters Y and K have been obtained by fitting calculated macroscopic crystal constants to the relevant experimental values. In addition, three-body bond-bending terms are used to model the directional character of covalent bonds:

$$V_B(\theta)=\tfrac{1}{2}k_B(\theta-\theta_0)^2 \ , \tag{2.3}$$

where k_B is the bond-bending force constant and θ_0 the equilibrium bond angle. Table I shows two different potential parameter sets appropriate for $LiNbO_3$. Model I has been obtained by combining empirical potential sets for Li_2O and Nb_2O_5 to give a $LiNbO_3$ potential model, whilst model II is the result of least-squares fitting to macroscopic properties of $LiNbO_3$. It is important to note that all $LiNbO_3$ potential models (including the above model I) which did not take shell-polarization effects explicitly into account have failed to reproduce the ferroelectric phase of $LiNbO_3$, because the Li ion always relaxed into the nearest oxygen plane, a situation corresponding to the paraelectric $R\,3c$ phase of $LiNbO_3$. Only after including shell coordinates as adjustable parameters in the fitting procedure (model II) were we able to reproduce the $R\,\bar{3}c$ (D_{3d}^6) phase of $LiNbO_3$. Thus, shell polarization turns out to be necessary in order to model ferroelectricity in $LiNbO_3$ crystals,[21] and with a suitable potential model, the minimum of the lattice energy with respect to all ionic core and shell displacements yields the equilibrium configuration of the perfect crystal. For this minimization procedure the computer code PLUTO[22] is used. Once the equilibrium configuration of the perfect lattice is obtained, defect energies are calculated using a two-region strategy, where the crystal relaxation around defects is fully taken into account. The inner region around the defect containing about 120 ions is treated atomistically. Polarization effects of the outer region are approximated by the Mott-Littleton approach.[23] All relevant defect energies have been calculated in this way using the computer code CASCADE.[24]

Although originally developed for ionic crystals such as alkali halides, the above simulation techniques have

TABLE I. $LiNbO_3$ potential parameters according to models I and II.

Interaction	A (eV)		ρ (Å)		C (eV Å^6)	
	I	II	I	II	I	II
O^{2-}-O^{2-}	22764.3	22764.3	0.149	0.149	27.879	27.879
Nb^{5+}-O^{2-}	1796.3	1113.3	0.34598	0.38815	0.0	0.0
Li^{+}-O^{2-}	262.5	816.3	0.34760	0.26086	0.0	0.0

Ion	Y/e		k (eV Å^{-2})	
	I	II	I	II
O^{2-}	−2.811	−4.656	103.07	462.04
Nb^{5+}	−4.496	4.022	1358.58	17.85
Li^{+}	0.0	0.0	∞	∞

Interaction	k_B (eV rad^{-2})		θ_0 deg	
	I	II	I	II
O-Nb-O		0.5776		90.0

been successfully applied to silicates[25] and other oxides[26,27] where a considerable degree of covalency is expected. It may be argued that covalency-related effects are to a certain extent absorbed in empirically obtained potential models.

III. RESULTS AND DISCUSSION

In Table II some elementary defect energies calculated with our two $LiNbO_3$ potential models are compared. The overall agreement is clear, although different approaches have been applied to obtain these sets of potentials.

It is worthwhile at this point to digress, and stress that within the chosen potential model, defect energies, and properties obtained from them, may be calculated to any degree of accuracy, being dependent only on the accuracy with which the parameters in the potential are input. Thus, it is valid to compare numbers which differ by only tenths of an electron-volt, in order to deduce the likely model for nonstoichiometry. Of course, the defect energies will be altered by changing the parameters in the potential model. However, when we did so in the present case, we found that, as expected, the *relative* energies were unchanged. This is an important point, and the reader is referred to Tomlinson *et al.*[21] for further discussion of the sensitivity of results to the potential model.

A. Schottky and Frenkel disorder in $LiNbO_3$

We begin our discussion of the intrinsic defect structure in $LiNbO_3$ by considering Schottky and Frenkel disorder according to the following reactions:

$$\text{“}LiNbO_3\text{”} \leftrightarrow Li_2O + 2V'_{Li} + V^{\cdot\cdot}_O \ , \tag{3.1}$$

$$\text{“}LiNbO_3\text{”} \leftrightarrow Nb_2O_5 + 2V^{5'}_{Nb} + 5V^{\cdot\cdot}_O \ , \tag{3.2}$$

$$\text{“}LiNbO_3\text{”} \leftrightarrow LiNbO_3 + V'_{Li} + V^{5'}_{Nb} + 3V^{\cdot\cdot}_O \ , \tag{3.3}$$

$$\text{“}LiNbO_3\text{”} \leftrightarrow V'_{Li} + Li^{\cdot}_I \ , \tag{3.4}$$

$$\text{“}LiNbO_3\text{”} \leftrightarrow V^{5'}_{Nb} + Nb^{5\cdot}_I \ , \tag{3.5}$$

$$\text{“}LiNbO_3\text{”} \leftrightarrow V^{\cdot\cdot}_O + O''_I \ . \tag{3.6}$$

The calculated Schottky and Frenkel formation energies per defect are summarized in Table III, where they are also compared with respective defect energies obtained in $BaTiO_3$.[5]

The results concerning Schottky disorder are very similar to those for $BaTiO_3$, i.e., all Schottky-type reactions yield comparable large formation energies per defect. In addition, their absolute values are the same order of magnitude as the formation energies of Schottky disorder in $BaTiO_3$, where this type of defect structure has been suggested to be insignificant. We suggest, therefore, that Schottky disorder is not important in the defect chemistry of $LiNbO_3$.

TABLE II. Some fundamental defect energies (in eV).

Defect	Model I	Model II
V''_O	21.7	19.5
V'_{Li}	7.9	9.8
$V^{5'}_{Nb}$	120.3	117.3
$Nb^{4\cdot}_{Li}$	−106.1	−99.5

TABLE III. Schottky and Frenkel formation energies (eV) per defect for $LiNbO_3$ and $BaTiO_3$.

$LiNbO_3$		$BaTiO_3$	
	(a) Schottky disorder		
Li_2O	1.94	BaO	2.58
Nb_2O_5	2.85	TiO_2	2.90
$LiNbO_3$	3.91	$BaTiO_3$	2.29
	(b) Frenkel disorder		
O^{2-}	3.42	O^{2-}	4.49
Nb^{5+}	6.26	Ti^{4+}	7.56
Li^+	0.93	Ba^{2+}	5.94

Because of its large formation energy, Nb Frenkel disorder will not occur in $LiNbO_3$, whereas Li Frenkel disorder is probably important due to the comparatively small Li binding energy and the existence of structural vacancy sites which are very similar to the cation sites. It may be that Li Frenkel defects are responsible for the observed ion conductivity in $LiNbO_3$ crystals (see Ref. 4 for further references). The measured activation energy of 1.1 eV supports this interpretation, since it is comparable with our calculated Li Frenkel-defect formation energy. From Table III it is further seen that for $BaTiO_3$ all types of Frenkel disorder are unfavorable, in contrast to $LiNbO_3$.

B. Defects resulting from nonstoichiometry

As we outlined in the Introduction the intrinsic defect structure of $LiNbO_3$ originates to a considerable extent from Li/Nb nonstoichiometry. Each defect model accounting for this nonstoichiometry has to obey experimentally confirmed conditions which may be stated as follows.

(1) There is essentially only Li_2O deficiency and no Li_2O excess.

(2) The density of $LiNbO_3$ increases with increasing Li_2O deficiency.

(3) The charge-compensating mechanism for Li_2O deficiency involves $V^{5'}_{Nb}$ and $Nb^{4\cdot}_{Li}$.[11]

First, we discuss what happens on the Li_2O-rich side of stoichiometric equilibrium. Essentially, three Li_2O solution reactions may be proposed:

$$\text{“}LiNbO_3\text{”} + Li_2O \leftrightarrow 2LiNbO_3 + 2V^{5'}_{Nb} + 5V^{\cdot\cdot}_O \ , \tag{3.7}$$

$$\text{“}LiNbO_3\text{”} + Li_2O \leftrightarrow LiNbO_3 + Li^{4'}_{Nb} + 2V^{\cdot\cdot}_O \ , \tag{3.8}$$

$$\text{“}LiNbO_3\text{”} + Li_2O \leftrightarrow 2Li^{\cdot}_I + O''_I \ . \tag{3.9}$$

From Table IV we see that reaction (3.9) is energetically preferred. However, this mode of accommodation of excess Li_2O suggests that the $LiNbO_3$ crystal lattice would

TABLE IV. Incorporation of excess Li_2O in $LiNbO_3$

Mode of Li_2O excess	Energy per Li_2O (eV)
Eq. (3.7)	17.66
Eq. (3.8)	5.82
Eq. (3.9)	4.71

change its identity to give another structure, possibly that of Li_3NbO_4. The large calculated energy per excess Li_2O (4.7 eV) supports this suggestion. In agreement with statement (1) our calculations show that Li_2O excess is not likely to occur in $LiNbO_3$.

Therefore, we may concentrate on Li_2O deficiency in $LiNbO_3$. We do this by discussing the most important defect models in terms of Li_2O out-diffusion:

$$\text{“}LiNbO_3\text{”} \leftrightarrow Li_2O + 2V'_{Li} + V^{\cdot\cdot}_{O} \ , \tag{3.10}$$

$$\text{“}LiNbO_3\text{”} \leftrightarrow 3Li_2O + 4V'_{Li} + Nb^{4\cdot}_{Li} \ , \tag{3.11}$$

$$\text{“}LiNbO_3\text{”} \leftrightarrow 3Li_2O + 4V^{5\prime}_{Nb} + 5Nb^{4\cdot}_{Li} \ . \tag{3.12}$$

Slight modification of (3.12) yields:

$$\text{“}LiNbO_3\text{”} \leftrightarrow 3Li_2O + 4(V^{5\prime}_{Nb}Nb^{4\cdot}_{Li})' + Nb^{4\cdot}_{Li} \ . \tag{3.13}$$

Table V contains our calculated results.

We find that the oxygen vacancy model (3.10) is energetically unfavorable. Thus Li_2O deficiency is compensated by formation of defects on the cation sublattice only. Considering the question of the increase in density of $LiNbO_3$ as Li_2O deficiency increases, it is apparent that Eqs. (3.11)–(3.13) all satisfy this criterion. To see this, we note that the oxygen sublattice is unaffected, so for each mole of $LiNbO_3$ consumed, excess niobium is effectively dissolved within the remaining $LiNbO_3$ by substitution at lithium sites. Thus, even though vacancies are formed, the mass per unit volume (density) will increase. For example, if (3.11) is the correct mechanism, for each out-diffusing Li_2O, the mass of $LiNbO_3$ increases by $\frac{1}{3}[(92.9-6.9)-(4\times 6.9)] \approx 19$ amu. Although models (3.12) and (3.13) would agree well with statements (2) and (3), they are unfavorable on energetic grounds. The energy difference between (3.13) and (3.11) amounts to about 6 eV per Li_2O. This result is not very surprising and has indeed qualitatively been suggested by Smyth.[6,13] The contradiction between calculated energies and the observation of Nb at Li sites in diffraction studies can be resolved if small regions in $LiNbO_3$ with an ilmenite-like stacking sequence exist. The crystal structures of ilmenite and $LiNbO_3$ are very similar and differ only by their cation staking sequence as shown schematically in Fig. 1. Our computer simulation shows that both $LiNbO_3$ modifications have similar stabilities. The lattice energy per unit cell of the ilmenite type is only 0.1 eV less favorable than the respective energy of perfect $LiNbO_3$. Thus, an intermixing of both structures in $LiNbO_3$ seems to be possible.

TABLE V. Modes of Li_2O out-diffusion in $LiNbO_3$.

Mode of Li_2O out-diffusion	Energy per Li_2O (eV)
Eq. (3.10)	5.82
Eq. (3.11)	4.56
Eq. (3.12)	15.17
Eq. (3.13)	10.67

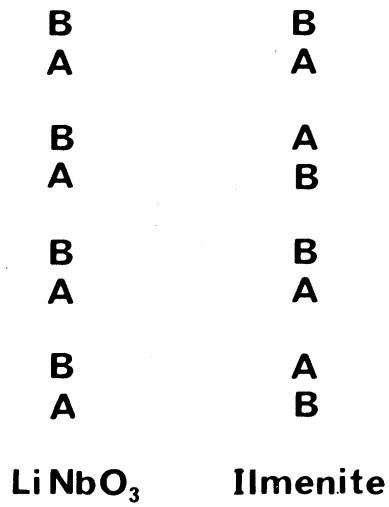

FIG. 1. Cation stacking sequences of ABO_3 oxides with $LiNbO_3$ and ilmenite structure.

Experimental evidence for ilmenite-like $LiNbO_3$ has been given by Kumada *et al.*, who reported the preparation of $LiNbO_3$ with the ilmenite structure using $NaNbO_3$ as a starting material.[28] Thus, we suggest that there are substantial intergrowths of an ilmenite stacking sequence in $LiNbO_3$, and that Li vacancies will preferentially occupy these regions.

C. Defects resulting from reduction of $LiNbO_3$

It is experimentally known that reduction of $LiNbO_3$ crystals is accompanied by increasing crystal density (however, the corresponding measurements have not been published until now[6]) and out-diffusion of O_2 and possibly Li_2O,[29,30] although the ratio $[Li_2O]/[O_2]$ is not known and will depend upon the crystal investigated. Basically two models for reduction of $LiNbO_3$ can be proposed. First, we consider the case of stoichiometric $LiNbO_3$. Because the $[Li_2O]/[O_2]$ ratio is not a critical parameter for the energy difference between both models, we may simplify the calculations by using one fixed (but principally arbitrarily chosen) ratio $[Li_2O]/[O_2]$ for the respective reduction models. The first model corresponds to the conclusions of Jorgensen and Bartlett:[9]

$$\text{“}LiNbO_3\text{”} \leftrightarrow O_2 + 2V^{\cdot\cdot}_{O} + 4e' \ . \tag{3.14}$$

This equation has to be combined with some mechanism for Li_2O out-diffusion; for example, we may write

$$\text{“}LiNbO_3\text{”} \leftrightarrow O_2 + Li_2O + 3V^{\cdot\cdot}_{O} + 2V'_{Li} + 4e' \ . \tag{3.15}$$

The second model according to Smyth[6,31,32] involves $Nb^{4\cdot}_{Li}$-antisite defects and reads

$$\text{“}LiNbO_3\text{”} \leftrightarrow O_2 + Li_2O + Nb_{Li}^{4\cdot} + 4e' \ . \tag{3.16}$$

Within both models e' represents a conduction-band electron. Our calculated results are summarized in Table VI. It is clearly seen that (3.14), whatever the Li_2O out-diffusion mode, is less favorable than the Smyth model (3.16). We note that this result is independent of the $LiNbO_3$ potential model used.

In the case of Li_2O-deficient $LiNbO_3$, model (3.16) may be reformulated by taking advantage of the intrinsic defect structure of $LiNbO_3$, i.e., Li vacancies within ilmenite regions.

We suggest three models depending on the degree of dissolving ilmenite intergrowths during the reduction process:

$$\text{“}LiNbO_3\text{”} + 2(Nb_{Li}^{4\cdot} V_{Nb}^{5'})' \leftrightarrow \tfrac{3}{2}O_2 + Nb_{Li}^{4\cdot} + 2(Nb_{Li}^{4\cdot} Li_{Nb}^{4'}) + 6e' \ , \tag{3.17a}$$

$$\text{“}LiNbO_3\text{”} + 2(Nb_{Li}^{4\cdot} V_{Nb}^{5'})' \leftrightarrow \tfrac{3}{2}O_2 + Nb_{Li}^{4\cdot} + (Nb_{Li}^{4\cdot} Li_{Nb}^{4'}) + 6e' \ , \tag{3.17b}$$

$$\text{“}LiNbO_3\text{”} + 2(Nb_{Li}^{4\cdot} V_{Nb}^{5'})' \leftrightarrow \tfrac{3}{2}O_2 + Nb_{Li}^{4\cdot} + 6e' \ . \tag{3.17c}$$

In the preceding equations we have represented lithium-deficient ilmenite regions as $(Nb_{Li}^{4\cdot} V_{Nb}^{5'})$ as shown in Fig. 2. Thus, the formation of electrons in the conduction band is due to the dissolution of ilmenite regions consequent upon Li out-diffusion from those regions. Equations (3.17) mean that all Li_2O molecules originating from (3.16) are used to fill up intrinsic defects by a reverse Li_2O out-diffusion process. Thus, we assume $[Li_2O]/[O_2]$ to be almost zero for Li_2O-deficient $LiNbO_3$ crystals. Now, reactions (3.17) in our favored ilmenite-structure intergrowth model will occur at an “internal surface” between the two regions. Whereas in (3.17a) the ilmenite structure remains stable during reduction, it is assumed to be at least partly dissolved in the reactions (3.17b) and (3.17c). Our calculated energies per electron are 1.7 eV for (3.17a), 0.96 eV for (3.17b), and 0.2 eV for (3.17c). We note that all versions of (3.17) are favored over the corresponding oxygen-vacancy model (3.14), for example, the energy difference between Eqs. (3.17a) and (3.14) amounts to about 0.6 eV per electron. Thus, on purely energetic grounds we would suggest dissolving of metastable ilmenite regions during reduction to be favored. However, Smyth *et al.*[33] have reported an enthalpy of about 6.1 eV per O_2 by measuring the O_2 out-diffusion as a function of temperature upon reducing a congruent $LiNbO_3$ sample under constant composition conditions. Dividing this enthalpy by 4, the number of liberated electrons per O_2, yields 1.52 eV per conduction-band electron which is in good agreement with Eq. (3.17a). Thus, by comparison with experiment we should think of the lithium vacancy rich ilmenite regions to be sufficiently stable to “survive” the reduction process according to reaction (3.17a). In addition, conductivity measurements performed at the same time confirm the electrons to be in conduction-band states during the experiment (i.e., trapping of electrons at intrinsic defects has not yet taken place), since the activation energy of about 0.54 eV corresponds to the mobility part only. A further reduction of the energy per electron to about 0.1 eV is achieved by using the important result of Sec. III D that bipolarons should represent the electronic ground state after reduction treatments.

In summary, our calculations suggest oxygen vacancies will not occur during reduction treatments of $LiNbO_3$; moreover, Li_2O-deficient crystals are predicted to be more easily reduced under suitable experimental conditions than stoichiometric crystals. Indeed experiments of Agulló-Lopez *et al.*[34] show the reduction process in stoichiometric samples to be weaker than in congruent crystals.

TABLE VI. Reduction models appropriate for $LiNbO_3$. Energies per electron are listed in eV. Model (3.14) has been combined with different modes of Li_2O out-diffusion.

Reduction model (3.14) combined with		Reduction model (3.16)
Eq. (3.10)	Eq. (3.11)	
3.74	3.43	2.80

D. Electronic structure, polarons, and bipolarons

Assuming the conduction band is associated with niobium ($4d$) orbitals and the valence band with oxygen

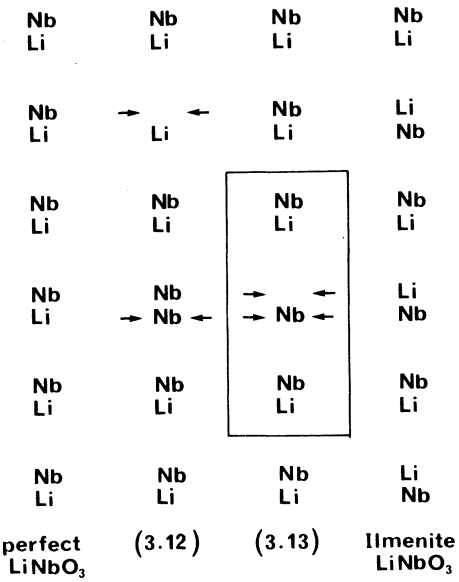

FIG. 2. Li_2O out-diffusion in $LiNbO_3$. The defects models (3.12) and (3.13) are visualized, and defects are denoted by arrows. For comparison, the stacking sequences of perfect and ilmenite $LiNbO_3$ are also shown. The frame in the third row is seen to be an ilmenite-like unit cell with Li vacancy (Ref. 13).

($2p$) orbitals, it is possible using our methods to calculate the thermal band gap in $LiNbO_3$. By combining electron and hole formation energies with the second electron affinity of oxygen and the fifth ionization energy of niobium, we calculate a value of 3.80 eV for the thermal band gap, which compares well with experimentally determined values of about 4 eV.[35] We have also studied the stability of electron polarons and electron bipolarons. Small polarons are predicted to be more favorable than large polarons assuming a conduction-band width Δ_{CB} of 2 eV. The stability condition for small polarons is given by

$$E_t(\mathrm{Nb}'_{\mathrm{Nb}}) < E_o(\mathrm{Nb}'_{\mathrm{Nb}}) - \frac{\Delta_{CB}}{2} . \tag{3.18}$$

$E_t(\mathrm{Nb}'_{\mathrm{Nb}})$ refers to the thermal formation energy of $\mathrm{Nb}'_{\mathrm{Nb}}$, i.e., all ionic cores and shells being relaxed, whereas $E_o(\mathrm{Nb}'_{\mathrm{Nb}})$ is the optical $\mathrm{Nb}'_{\mathrm{Nb}}$ formation energy calculated by allowing shell (i.e., electron) relaxation only. The right-hand side of Eq. (3.18) means that large polarons are stabilized by the half-conduction-band-width corresponding to electron delocalization.

Thus, according to our results electron conduction should be explained using the small-polaron model including some hopping mechanism. This finding seems to be in good agreement with conductivity measurements.[29,36]

In Table VII (b) calculated electron and hole trapping energies are summarized. It is seen that electrons are only weakly bound at oxygen vacancies. Thus, oxygen vacancies would be doubly ionized, as is the case for $BaTiO_3$.[5] Resulting from Li_2O deficiency and reduction, $\mathrm{Nb}^{4\cdot}_{\mathrm{Li}}$-antisite defects are expected to occur in $LiNbO_3$ with a concentration greater than 1%. Moreover, our calculations suggest $\mathrm{Nb}^{4\cdot}_{\mathrm{Li}}$ antisites to act as deep electron traps. These results suggest that the observed Nb^{4+} ESR in reduced $LiNbO_3$ stems essentially from $\mathrm{Nb}^{3\cdot}_{\mathrm{Li}}$-antisite defects, because these produce the lowest-lying single-polaron levels. However, single polarons are only detected by electron spin resonance after irradiating the reduced crystal samples. Thus, there must be a deeper diamagnetic ground-state level which is also polaronic in nature. Our calculations indicate that this ground-state level originates from bipolarons. We have simulated different bipolaron configurations such as $\mathrm{Nb}'_{\mathrm{Nb}}$-$\mathrm{Nb}'_{\mathrm{Nb}}$ and $\mathrm{Nb}^{3\cdot}_{\mathrm{Li}}$-$\mathrm{Nb}'_{\mathrm{Nb}}$ using the CASCADE code. Covalency contributions to the binding energy were added to the defect energies obtained in this way by considering transition matrix elements between $d_{3z^2-r^2}$ orbitals at each Nb^{4+} partner of the bipolaron [see Table VII(a)]. From ESR[37] it is known that the ground state at a single Nb^{4+} ion in $LiNbO_3$ is of this $d_{3z^2-r^2}$ type. Calculating the transition matrix elements by the method of Harrison (Ref. 38 and the Appendix of the present paper) an additional stabilization energy due to covalency of about 1 eV is obtained. We find that bipolarons are stable as $(\mathrm{Nb}'_{\mathrm{Nb}}\mathrm{Nb}^{3\cdot}_{\mathrm{Li}})^{2\cdot}$ defect pairs (normal site-antisite pairs) oriented along the crystal c axis because the covalent energy gain is largest for this configuration. It should be noted that the electrons in this defect can be considered as being stabilized by the donor-acceptor nature of the pair. It is emphasized that each isolated $\mathrm{Nb}^{4\cdot}_{\mathrm{Li}}$-antisite defect existing as part of the intrinsic defect structure has a $\mathrm{Nb}_{\mathrm{Nb}}$ neighbor; thus the formation of normal site-antisite bipolarons upon reduction simply means filling up these Nb pairs with electrons. $(\mathrm{Nb}'_{\mathrm{Nb}}\mathrm{Nb}'_{\mathrm{Nb}})^{2'}$ bipolarons as well as the Anderson bipolaron, i.e., $\mathrm{Nb}''_{\mathrm{Nb}}$ or $\mathrm{Nb}^{2\cdot}_{\mathrm{Li}}$, seem to be unlikely in $LiNbO_3$ because they are not able to produce electronic energy levels lying below the $\mathrm{Nb}^{3\cdot}_{\mathrm{Li}}$-related levels. The latter result concerning Anderson bipolarons is also confirmed experimentally, because Nb^{3+} would probably have been detected by ESR spectroscopy.

Finally Table VII(b) contains some hole trapping energies. Although hole trapping at Nb vacancies would be energetically favored, we consider trapping to occur at Li vacancies, since according to our defect model Nb vacancies are not significant. Agulló-Lopez *et al.*[17] have estimated an activation energy of about 0.54 eV for thermal decay of the 500-nm optical-absorption band induced by x-ray irradiation at low temperatures assuming first-order kinetics. Schirmer and von der Linde[37] suggested this 500-nm absorption band to stem from holes trapped at Li vacancies. Such an interpretation is in good agreement with our calculated hole trapping energy of 0.44 eV, which is of the same order of magnitude as the measured activation energy.

TABLE VII. (a) Calculation of bipolaron energies. Calculation of binding energies (including covalency): $(\mathrm{Nb}'_{\mathrm{Nb}}\mathrm{Nb}^{3\cdot}_{\mathrm{Li}})^{2\cdot} \rightarrow \mathrm{Nb}'_{\mathrm{Nb}} + \mathrm{Nb}^{3\cdot}_{\mathrm{Li}}$, -1.66 eV; $(\mathrm{Nb}'_{\mathrm{Nb}}\mathrm{Nb}'_{\mathrm{Nb}})^{2'} \rightarrow 2\mathrm{Nb}'_{\mathrm{Nb}}$, -0.55 eV. (b) Some electron and hole trapping energies (in eV).

(a)

Defect	Defect formation energy (eV)
$\mathrm{Nb}^{3\cdot}_{\mathrm{Li}}$	-55.58 (CASCADE)
$\mathrm{Nb}'_{\mathrm{Nb}}$	$+45.37$ (CASCADE)
$(\mathrm{Nb}'_{\mathrm{Nb}}\mathrm{Nb}^{3\cdot}_{\mathrm{Li}})^{2\cdot}$	-10.87 (CASCADE) including covalency: -11.87
$(\mathrm{Nb}'_{\mathrm{Nb}}\mathrm{Nb}'_{\mathrm{Nb}})^{2'}$	$+91.19$ (CASCADE) including covalency: $+90.19$

(b)

Defect center (including trapped charge carrier)	Trapping energy (eV)
$V^{\cdot\cdot}_{O}$	-0.16
$\mathrm{Nb}^{3\cdot}_{\mathrm{Li}}$	-1.40
$(\mathrm{Nb}^{3\cdot}_{\mathrm{Li}}\mathrm{Nb}'_{\mathrm{Nb}})^{2\cdot}$	-1.66
$(\mathrm{Nb}'_{\mathrm{Nb}}\mathrm{Nb}'_{\mathrm{Nb}})^{2'}$	-0.55
$\mathrm{Nb}'_{\mathrm{Nb}}$	$+0.29$
$\mathrm{Nb}^{2\cdot}_{\mathrm{Li}}$	-0.59
V^{0}_{Li}	-0.44
$V^{4'}_{\mathrm{Nb}}$	-0.81

IV. CONCLUSIONS

Using a semiempirical theory (shell model and Mott-Littleton approximation), we are able to explain the in-

trinsic defect structure of $LiNbO_3$ consistently. The crystal relaxation around defects has been fully taken into account. Nb_{Li}-antisite defects and Li-cation vacancies are predicted to be the main defects compensating for Li_2O deficiency and reduction treatments. Small crystal regions with ilmenite-like stacking sequence seem to be probable in $LiNbO_3$. We argue that Li vacancies will preferentially segregate to ilmenite-like $LiNbO_3$.

In addition, we find oxygen vacancies are energetically unfavorable. Small polarons and bipolarons (normal site-antisite pairs) have been shown to be likely. These results support the model of Schirmer *et al.*[18] that the optical-absorption band at 500 nm occurring after reduction originates from bipolarons and not from oxygen vacancies. Finally, we note that the electron-irradiation experiments performed by Agulló-López *et al.*[19,24] can be explained by the intrinsic Nb_{Li}^{4}-antisite defects, which are always present. Oxygen displacement damage induced by electron irradiation will force the oxygen ions to release their additional electrons to conduction-band states because V_O as well as O_I are only shallow electron traps. Subsequent electron trapping at antisite defects leads to the formation of bipolarons which are probably responsible for the 500-nm optical-absorption band.

ACKNOWLEDGMENTS

We would like to thank Dr. M. Leslie for useful discussions.

APPENDIX: ESTIMATION OF COVALENCY CONTRIBUTIONS IN BIPOLARONS

In order to estimate covalent energy terms in bipolaron configurations we use a simple argument by Harrison.[38] The idea is to represent electronic states of solids by linear combinations of atomic orbitals and to assume the neighbor coupling matrix elements, i.e., the transfer matrix elements, to be simple functions of the neighbor distance:

$$\langle\alpha|H|\beta\rangle \propto \frac{1}{d^{r(l_\alpha,l_\beta)}} , \tag{A1}$$

where $r(l_\alpha,l_\beta)$ is a rational number depending on the respective angular-momentum quantum numbers l_α and l_β of the orbitals $|\alpha\rangle$ and $|\beta\rangle$. Originally $|\alpha\rangle$ and $|\beta\rangle$ have been considered to be s or p orbitals. In this case the number $r(\equiv 2)$ and the proportionality constant in (A1) have been found by equating band energies from linear combination of atomic orbitals (LCAO) theory and free-electron theory. Thereafter muffin-tin and pseudopotential theory have brought an extension to d orbitals.

It is observed by Harrison[38] that the above solid-state matrix elements give a very good semiquantitative account of the occupied states of homopolar molecules. Our bipolaron problem is simplified by considering covalency to occur only between neighboring Nb^{4+} ions, whereas the remainder of the crystal lattice serves to stabilize the highly charged Nb^{4+}-Nb^{4+} molecule. It is realistic to assume the spacing d between the Nb ions to be close to 3 Å; thus Nb orbitals are, to a good approximation, almost orthogonal. The covalent energy between $3z^2-r^2$ d orbitals along their common z axis ($\equiv$ crystal c axis) is then given by

$$V_{dd\sigma} = -\eta_{dd\sigma}\frac{\hbar^2 r_d^3}{m_e d^5} . \tag{A2}$$

After inserting the universal Harrison parameter $\eta_{dd\sigma} = -16.2$ and $r_d(\mathrm{Nb}) = 1.28$ Å we obtain

$$V_{dd\sigma}(\mathrm{Nb}-\mathrm{Nb}) \simeq 1 \text{ eV} . \tag{A3}$$

Finally, we emphasize that this calculation is, of course, not exact. Rigorous calculations should be performed by combining a quantum-mechanical treatment of a cluster containing the respective defects and near ions with self-consistent polarization in the surrounding perfect lattice as described by the shell model. However, the calculation gives a reasonable estimate of the relative importance of covalent stabilization of $(Nb'_{Nb}Nb^{3\cdot}_{Li})^{2\cdot}$ pairs.

[1]J. G. Bergman *et al.*, Appl. Phys. Lett. **12**, 92 (1968).
[2]J. E. Midwinter, J. Appl. Phys. **39**, 3033 (1968).
[3]E. H. Turner, F. R. Nash, and P. M. Bridenbaugh, J. Appl. Phys. **41**, 5278 (1970).
[4]A. Räuber, in Vol. 1 of *Current Topics in Material Science*, edited by E. Kaldis (North-Holland, Amsterdam, 1978), p. 481.
[5]G. V. Lewis and C. R. A. Catlow, J. Phys. Chem. Solids **47**, 89 (1986).
[6]D. M. Smyth, Prog. Solid State Chem. **15**, 145 (1984).
[7]H. Yamada and G. R. Miller, J. Solid State Chem. **6**, 169 (1978).
[8]H. Fay, W. J. Alford, and H. M. Dess, Appl. Phys. Lett. **12**, 89 (1968).
[9]P. J. Jorgensen and R. W. Bartlett, J. Phys. Chem. Solids **30**, 2639 (1969).
[10]P. Lerner, C. Legras, and J. P. Duman, J. Cryst. Growth **3/4**, 231 (1968).
[11]S. C. Abrahams and P. Marsh, Acta Crystallogr. Sect. B **42**, 61 (1986).
[12]G. E. Peterson and A. Carnevale, J. Chem. Phys. **56**, 4848 (1972).
[13]D. M. Smyth (unpublished).
[14]K. L. Sweeney and L. E. Halliburton, Appl. Phys. Lett. **43**, 336 (1983).
[15]J. L. Ketchum, K. L. Sweeney, L. E. Halliburton, and A. F. Armington, Phys. Lett. **94A**, 450 (1983).
[16]L. E. Halliburton, K. L. Sweeney, and C. Y. Chen: Nucl. Instrum. Methods Phys. Res. B **1**, 344 (1984).
[17]L. Arizmendi, J. M. Cabrera, and F. Agulló-López, J. Phys. C **17**, 515 (1984).
[18]O. F. Schirmer, S. Juppe, J. Koppitz, Cryst. Lattice Defects Amorph. Mater. **16**, 353 (1987).
[19]E. R. Hodgson and F. Agulló-López, Solid State Commun. **64**, 965 (1987).
[20]B. G. Dick and A. W. Overhauser, Phys. Rev. **112**, 90 (1958).

[21]S. M. Tomlinson, C. M. Freeman, C. R. A. Catlow, H. Donnerberg, and M. Leslie, J. Chem. Soc. Faraday Trans. 2, **85**, 367 (1989).
[22]C. R. A. Catlow and M. J. Norgett, Atomic Energy Research Establishment Harwell Report No. M2763, 1978 (unpublished).
[23]N. F. Mott and M. J. Littleton, Trans. Faraday Soc. **34**, 485 (1938).
[24]M. Leslie, Solid State Ionics **8**, 243 (1983).
[25]S. C. Parker and G. D. Price, Physica B+C **131B**, 290 (1985).
[26]G. V. Lewis and C. R. A. Catlow, J. Phys. C **18**, 1149 (1985).
[27]C. R. A. Catlow, C. M. Freeman, M. S. Islam, R. A. Jackson, M. Leslie, and S. M. Tomlinson, Philos. Mag. A **58**, 123 (1988).
[28]N. Kumada, N. Ozawa, F. Muto, and N. Kinomura, J. Solid State Chem. **57**, 267 (1985).
[29]R. Courths, P. Steiner, H. Höchst, and S. Hüfner, Appl. Phys. **21**, 345 (1980).
[30]I. P. Kaminow and J. R. Carruthers, Appl. Phys. Lett. **22**, 326 (1973).
[31]D. M. Smyth, Ferroelectrics **50**, 93 (1983).
[32]H. M. Chan, Z. Zhuang, and D. M. Smyth (unpublished).
[33]D. M. Smyth (unpublished).
[34]A. Garcia-Cabanes, C. Zaldo, J. A. San-Garcia, J. M. Cabrera, and F. Agulló-López, Phys. Rev. B **37**, 6085 (1988).
[35]D. Redfield and W. J. Burke, J. Appl. Phys. **45**, 4566 (1974).
[36]P. Nagels, in *The Hall Effect and Its Applications,* edited by C. L. Chien and C. R. Westlake (Plenum, New York, 1980).
[37]O. F. Schirmer and D. von der Linde, Appl. Phys. Lett. **33**, 35 (1978).
[38]W. A. Harrison, *Electronic Structure and the Properties of Solids* (Freeman, San Francisco, 1980).